DAMAGE TOLERANCE ANALYSIS AND TESTING OF THE FIGHTER AIRCRAFT 37 VIGGEN

Björn Palmberg, Mats-Olof Olsson, Per-Olof Boman and Anders F. Blom

Structures Department
The Aeronautical Research Institute of Sweden (FFA)
P.O. Box 11021, S-161 11 Bromma, Sweden

Abstract

The swedish fighter aircraft 37, Viggen, designed some 25 years ago on a safe life basis, has been re-assessed in terms of a damage tolerance evaluation. In particular, four versions of the main wing attachment frame and some components in the fin have been subjected to both detailed analyses and damage tolerance testing.

Because of the original safe life design, resulting in rather high stresses, very extensive FE-analyses have been necessary to perform in order to get accurate stress distributions in critical sections for subsequent evaluation of 3-D stress intensity factors. Also, high demands have been placed on the accuracy of the crack growth predictions and, thus, extensive validation of the crack growth prediction technique has been required.

Structural testing, with artificial initial flaws, have been carried out with the aim of obtaining crack growth data for correlation to the prediction technique. The stress analyses were mainly verified on basis of traditional static and fatigue testing results available from the design phase of the aircraft.

It is concluded that the methodology used is state of the art and that it has been successfully verified. Furthermore, damage tolerance of the aircraft has been analytically proven and experimentally verified. Finally, extension of the original design life may be possible following further considerations.

Introduction

The swedish fighter aircraft 37 Viggen, Figure 1, designed some 25 years ago on a safe life basis, has been re-assessed in terms of a damage tolerance evaluation. The aim has been to ensure structural safety, and to investigate the possibilities for extending the original life of the aircraft. The scope, sofar, has been to make a complete assessment of four versions of the main wing attachment frame and the fighter version of the fin.

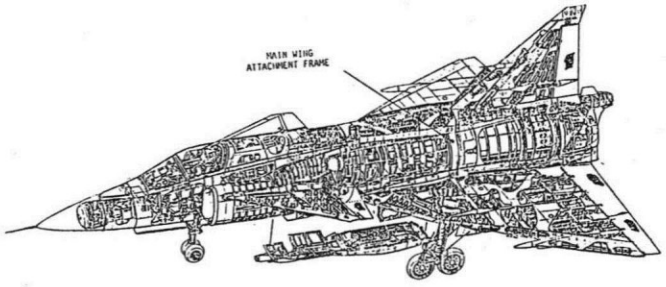

Figure 1. Fighter aircraft JA 37 "VIGGEN"

The principal geometry of the main wing attachment frame is shown in Figure 2. The frame can simplified be described as an assemblage of two curved U- or I-shaped beams, located a distance of 160.0 mm apart and kept together by inner and outer cover sheets. The beams (frames) are made of an aluminium die forging and the cover sheets are also made of an aluminium alloy. Between the two frames (beams) a structural detail, called middle part, is located as indicated in Figure 2. Also, a lower rear engine attachment is mounted between the two frames, see Figure 2.

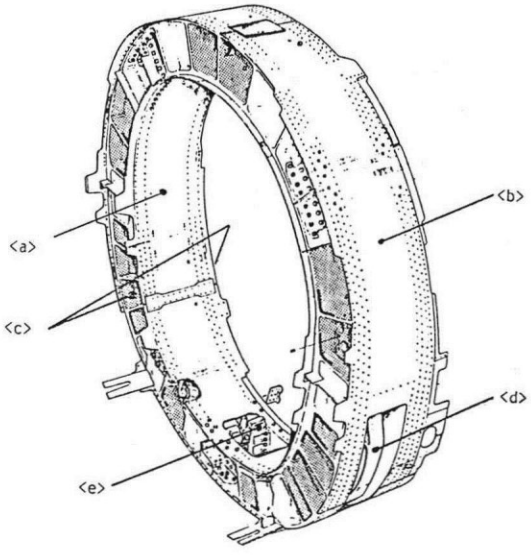

Figure 2. Main wing attachment assemblage. Principal parts are : <a> inner cover sheet, <b> outer cover sheet, <c> forward and aft frame forgings, <d> middle part and <e> rear engine attachment

The four versions of the frame differ essentially with respect to thicknesses in the webs and the flanges but also with respect to sheet thicknesses and diameters of some major holes. Two of the versions studied are used in the attack version of the aircraft (AJ) while the other two are used in the fighter version (JA). In both cases the existance of two versions for each aircraft type is due to major changes in the geometry of the frames made after serial production of several aircraft.

The main wing attachment frame is loaded by the main wing spar. It is the only attachment frame that takes up the bending moment from the wings. Shear loads are distributed on several frames. The loads from the main wing spar are introduced into two attachment holes of each frame (beam) and two holes of the middle part. The purpose of the middle part, which depending on version is made of an aluminium die forging or a high strength steel forging, is to distribute some of the load to two more attachment holes in the frame, called middle part holes. Furthermore, the main wing attachment frame is loaded by the engine through the rear engine attachment, which transfers vertical loads, and from the rest of the fuselage through the cover sheets. A principal sketch of the loads acting on a quarter of an isolated main wing attachment frame assemblage is shown in Figure 3. The load, P1z, at the top of the frame is introduced in combination with extra loads on the engine attachment to compensate for the missing load transfer from the rest of the fuselage when an isolated assemblage is studied. Naturally, the magnitudes of the loads on the different versions of the main wing attachment frame are different.

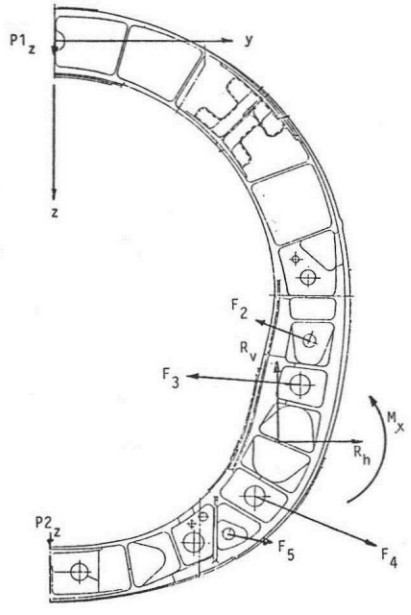

Figure 3. Schematic showing the loads applied. The loading is proportional, meaning that the time history is described by one single parameter. (R_h, R_v and M_x are resultants of the attachment loads)

The complete JA fin, shown in Figure 4, has to a large extent been analyzed and tested in an early phase of the project. During the phase presented in this paper attention was payed to the main and forward attachments as well as to rudder hinges.

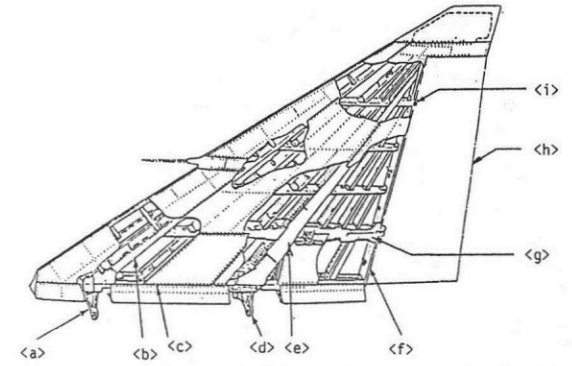

Figure 4. Location of different component in the JA 37 fin. <a> Forward attachment. <b> Forward spar. <c> Root rib. <d> Main attachment. <e> Main spar. <f> Rear spar. <g> Lower hinge. <h> Rudder. <i> Upper hinge

The aim of this paper is to summarize the performed damage tolerance analyses and testing for the newest fighter version of the aircraft. In particular, the main wing attachment frame and the forward fin attachment will be discussed. The principal geometry of the latter is shown in Figure 5.

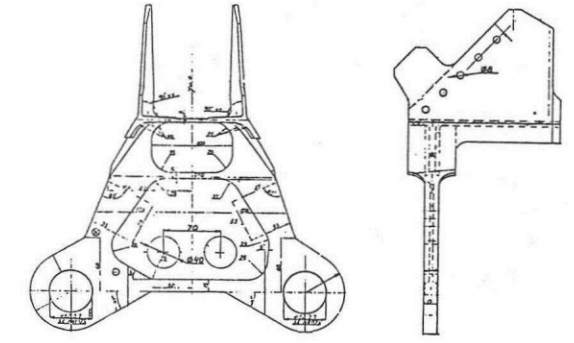

Figure 5. Geometry of JA 37 forward fin attachment

Damage Tolerance Assessment

The approach taken has been to follow the military specification MIL-A-83444 issued by the United States Air Force /1/. All of the components considered represent primary structures with few or no alternative load paths and have therefore been classified as slow crack growth structures. Initial flaw size assumptions follow the requirements of the specification /1/. A conservative residual strength requirement of 1.2 times limit load has been applied in terms of the linear

elastic plane strain fracture toughness, KIc, irrespective of actual thicknesses, except for cover sheets where Kc values for actual thicknesses were used.

Load Spectra and Stress Analyses

The load spectrum used for both analytical predictions and for testing of some coupon test specimens and an isolated main wing attachment frame assemblage is shown in Figure 6. As can be seen, the utilized design spectrum is more severe than the average spectrum for the usage of the aircraft. The design load spectrum for the fin is shown in Figure 7. The aircraft is not equipped with gauges for direct evaluation of actual loading of the fin, hence, a comparison between the design spectrum and the spectrum for actual usage is not possible to make.

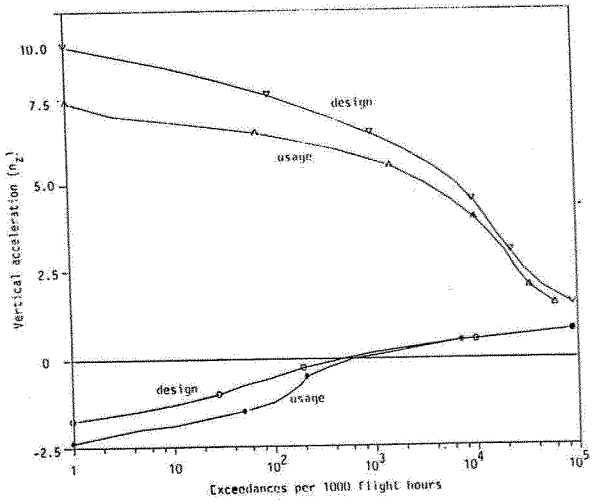

Figure 6. Comparison between design spectrum and in-flight recorded spectrum for the average aircraft

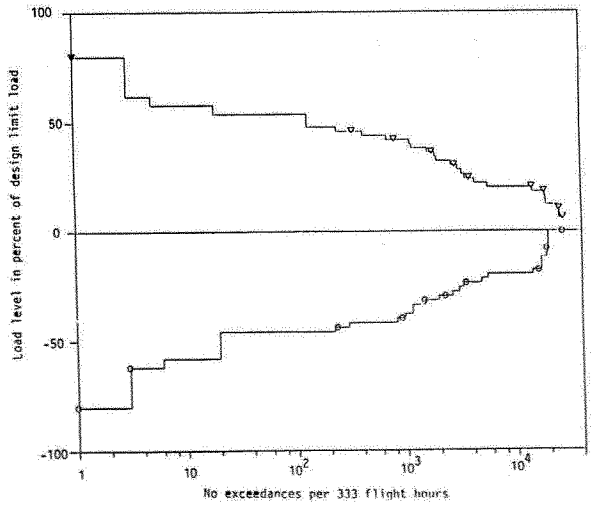

Figure 7 Test spectrum for forward fin attachment

The finite element (FE) analyses have been made in several steps where the first step in each analysis has been to make a global model of the complete component. These global models were able to describe stiffnesses correctly and to indicate where stress concentrations were located. In a few cases the global models were sufficienly detailed to give local stresses but usally more detailed models were required. A typical example of a global model for a quarter of the main wing attachment frame assemblage (remaining after accounting for the symmetry) is shown in Figure 8. The model, which is made using a substructuring technique, consists of approximately 75000 degrees of freedom.

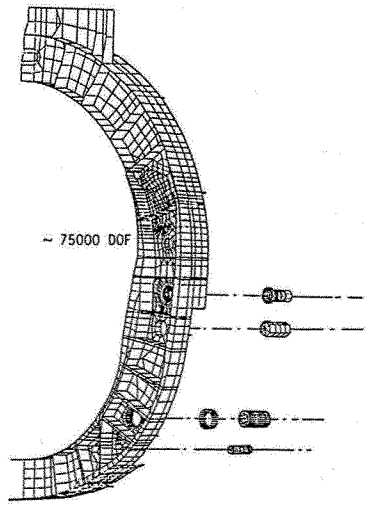

Figure 8. FE-model. Due to symmetry only 1/4 of the real structure is modelled

Based on the global FE-results, critical areas were identified, which were then subjected to more detailed FE-analyses, including such elements as accounting for bushings and solving contact problems. The boundary conditions for the detailed models were obtained from the global models in terms of displacements and rotations of nodes along the created cuts through the global models.

The region around the fuel pipe holes in the main wing attachment frame, see Figure 9, were analyzed using the p-version of a newly developed self-adaptive FE-code /2/. Also, some stress intensity factors were computed using this technique, which is believed to be the most accurate technique there is for such calculations.

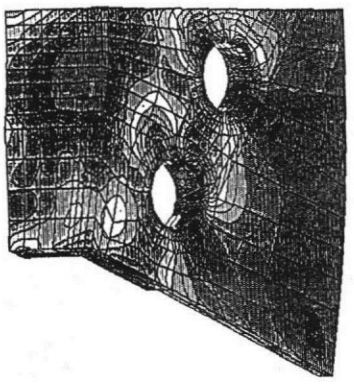

Figure 9. Stress analysis of fuel pipe holes using p-version of self adaptive FE-code

Regions around major attachment holes were analyzed using coventional FE-technique but, as already mentioned, contact stresses between wing bolts and bushings as well as between bushings and frame forgings were computed using automatic iterative solutions. The detailed analyses were in many cases repeated with considerations of more and more details, such as heads of bolts and stiffening effects of middle parts. The reasons for repeating the detailed analyses were seemingly improper or too large deformations and unrealistically high local stresses. For example, by including the bolt head in the model of the middle part hole region, see Figure 10, the largest principal stress was reduced by 25% due to reduced bolt tilting.

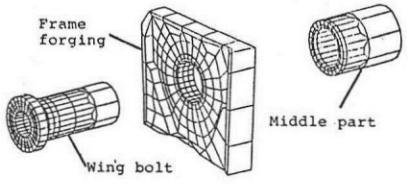

Figure 10. FE-model of middle part bolt, including bolt head and regions of the frame forging and the middle part

Fracture Mechanics and Fatigue Crack Propagation

A difficulty in the damage tolerance analysis has been to obtain relevant stress intensity factors. In many cases the stresses at critical locations have been high (locally) with large gradients in both surface and thickness directions. Stress intensity factor solutions based upon a remotely applied uniform loading are generally not able to describe the local stress gradients. Besides, it is very difficult to define the remote uniform loading.

The most accurate stress intensity factors are those computed with the adaptive FE-technique, see Figure 11. However, there are too many critical locations for applying this technique everywhere.

Second best stress intensity factor solutions seem to be those based upon the weight function technique, in which case local stress distributions can be described accurately. Such stress distributions were obtained directly from the FE-analyses and they are valid as long as no major changes due to load re-distributions occur. However, weight functions for 3D geometries are scarce. For 2D geometries it is more easy to find accurate weight functions but through the thickness cracks were, in general, a far too severe assumption for the critical locations studied.

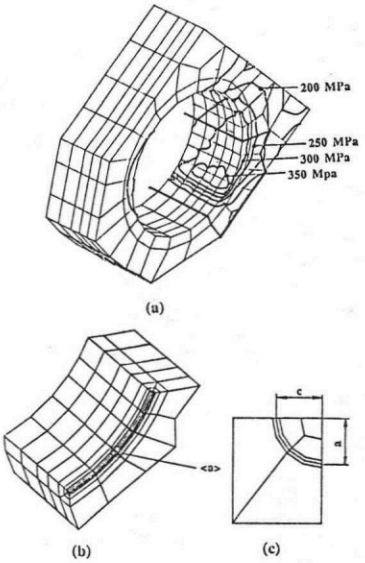

STRIPE results, uniform p=6			
a (mm)	c (mm)	K_{Ia} (MPa√mm)	K_{Ic} (MPa√mm)
1.3	1.3	472.8	572.5
2.0	2.6	621.9	749.2
2.0	3.0	647.4	778.8
1.3	1.6	514.6	602.9

(d)

Figure 11. K_I determination using p-version FE-method, ref /2/. (a) Stress results for lower wing bolt hole (b) Local model with boundary displacements and contact pressure distribution from the global analyses. The location of the crack is indicated by <a> (c) Shows the crack geometry and (d) is a table showing the results for four different crack sizes. (a=c=1.3 corresponds to the assumed initial flaw size according to ref /1/

The solution to the problem was to introduce correction functions such that the 2D solutions could be modified into approximative 3D solutions, considering the local stress distribution in just one direction and assuming that this stress distribution was uniform in the second direction.

Fatigue crack growth predictions were performed using a cycle-by-cycle analysis technique without consideration of plasticity induced load interac-

tion effects. However, a method for extracting contributing load cycles from an irregular load sequence was used which can be described as a very simplified rain flow counting algorithm.

All available fracture mechanics and crack growth data for the aluminium alloys and the high strength steels involved have been critically reviewed and collected in a data base for easy access. Complementary testing on coupon specimen level was performed to derive constant amplitude fatigue crack growth data in cases where data were lacking. Figure 12 illustrates the collected data for one of the relevant aluminium alloys.

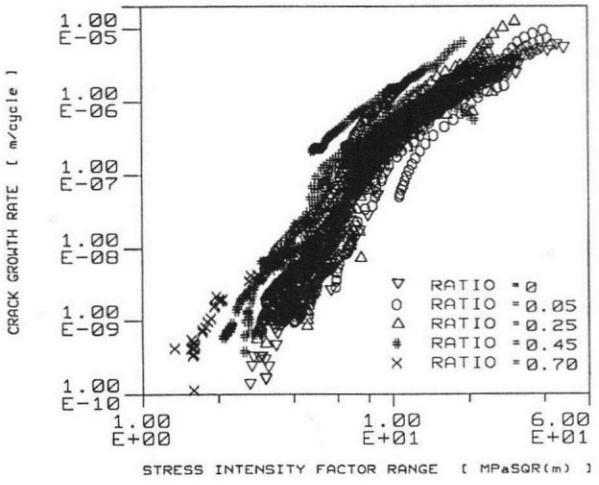

Figure 12. Fatigue crack growth rate data for a 7075 type of alluminium alloy. Ratio is equal to R, stress ratio.

Verification of Stresses and Crack Growth Prediction Technique

Firstly, the FE stress analyses were verified through comparisons to experimental results obtained during traditional static testing and fatigue testing of the components considered. The comparisons showed that stresses, in general, were computed very accurately even with the global models. Unfortunately, stresses really close to attachment holes could not be assessed due to lack of experimental data.

Secondly, the technique of modifying 2D stress intensity factors, based upon weight functions, into 3D solutions was verified by comparing such stress intensity factor solutions to solutions obtained using the adaptive FE-technique for a number of typical geometries.

Thirdly, the computer programme LIFE, used for the crack growth predictions, was verified as far as possible by comparisons to other computer programmes (CRACKS IV, ESACRACK, EFFGRO, etc) and to experimental results (on a coupon specimen level with wellknown stress intensity fator solutions) from the literature as well as from test results (on a coupon specimen level) obtained in the current investigation. These comparisons involved both constant amplitude results and results from different load spectra.

Structural Testing

The main wing attachment frame assemblage mounted in the test rig is shown in Figure 13. Due to relatively large displacements (wing root bending moments of up to 520 kNm are applied) the effective test frequency became around 0.2 Hz (testing was conducted at a constant displacement rate).

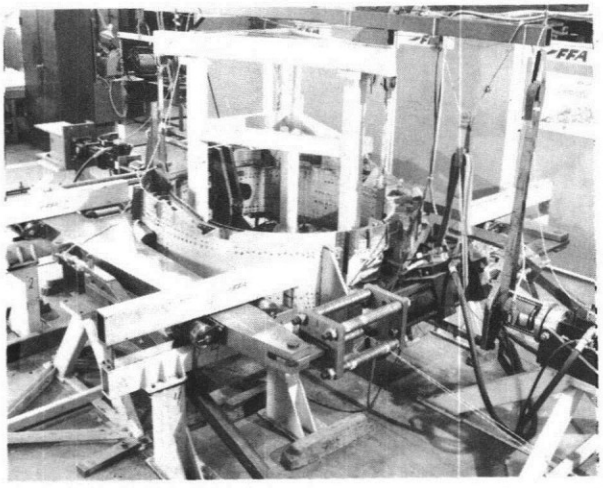

Figure 13. Test set-up for fatigue testing of an isolated main wing attachment frame assemblage

The actual frame tested had already been subjected to four fatigue lives of spectrum loading during the traditional testing to support the original safe life design of 2800 flight hours. No fatigue cracks were reported after the traditional testing. In the present investigation another four fatigue lives were applied subsequent to introduction of defects in the frame. A total of 22 artificial flaws (crack tip radius <0.02 mm), see example in Figure 14, were introduced by sawing in critical locations of the frame.

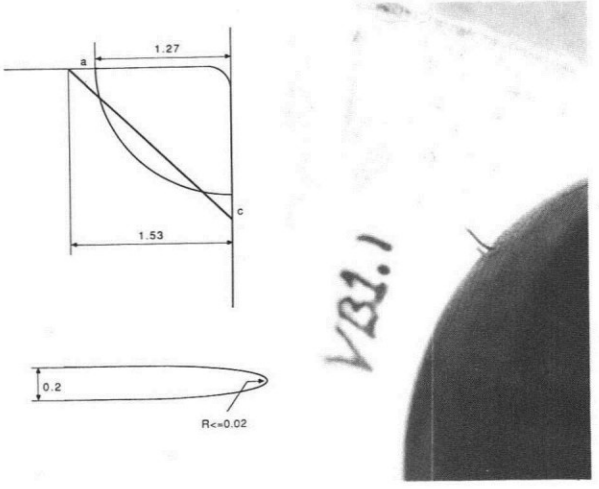

Figure 14. Sawcut with a=c=1.53 mm simulating a quarter-elliptical crack with a=c=1.27 mm

The locations chosen for saw cuts were selected on bases of the FE results, a strain survey using a brittle coating technique, crack growth predictions and inspection considerations. Very good agreement was found between the brittle coating results and the global finite element analysis both with respect to magnitudes and with respect to critical locations, see Figure 15.

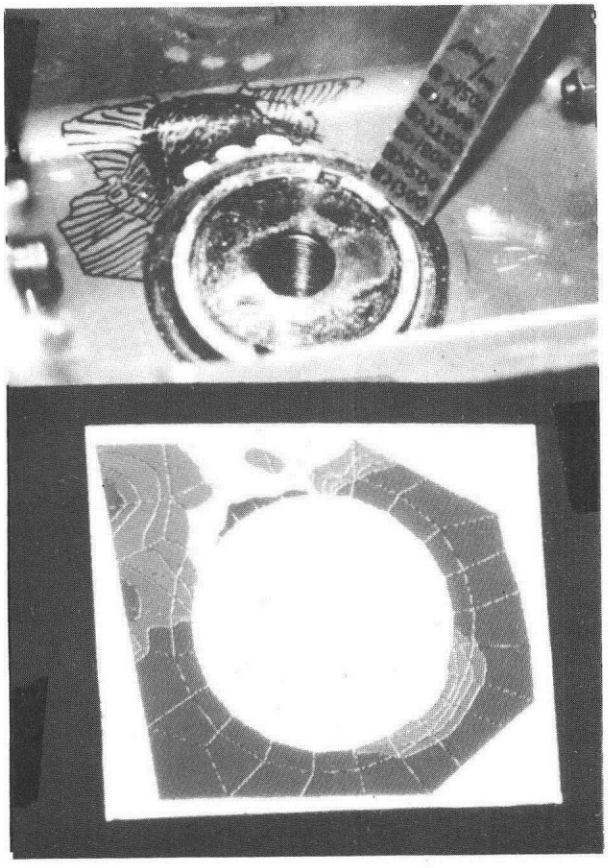

Figure 15. Comparison of brittle lacquer and FEM results

Crack growth was monitored both visually and by means of various NDI- techniques, primarily eddy current. Firstly, cracks started to grow from defects introduced at the two fuel pipe holes. This growth is easily observed visually and has therefore been very useful in verifying the analytical crack growth predictions. A comparison of predicted and experimentally observed crack growth at the small fuel pipe hole is shown in Figure 16.

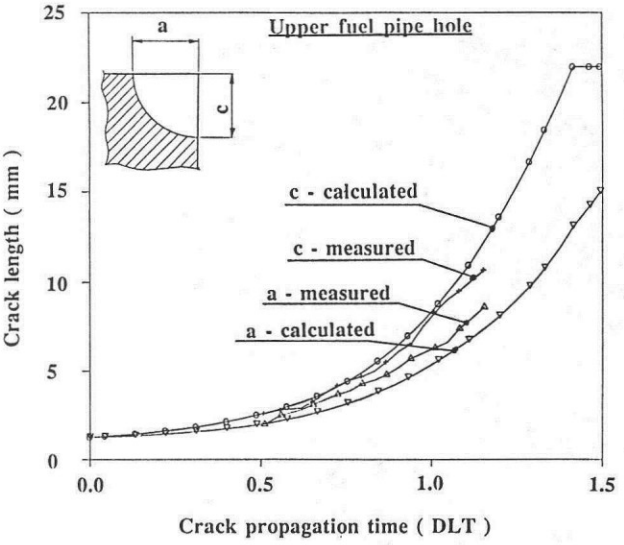

Figure 16. Comparison between predicted and measured crack length as function of time (design lifetimes)

Later on, after approximately 12500 simulated flight hours, these cracks resulted in final failure of the frame, as shown in Figure 17. After some 4000 simulated flight hours, crack growth was observed at one of the wing bolt holes. This is, according to numerical predictions, one of the most critical locations in the frame. However, as discussed further below, the predictions for this location are assumed to be overly conservative as friction between the interference fitted bushing and the frame forging was disregarded.

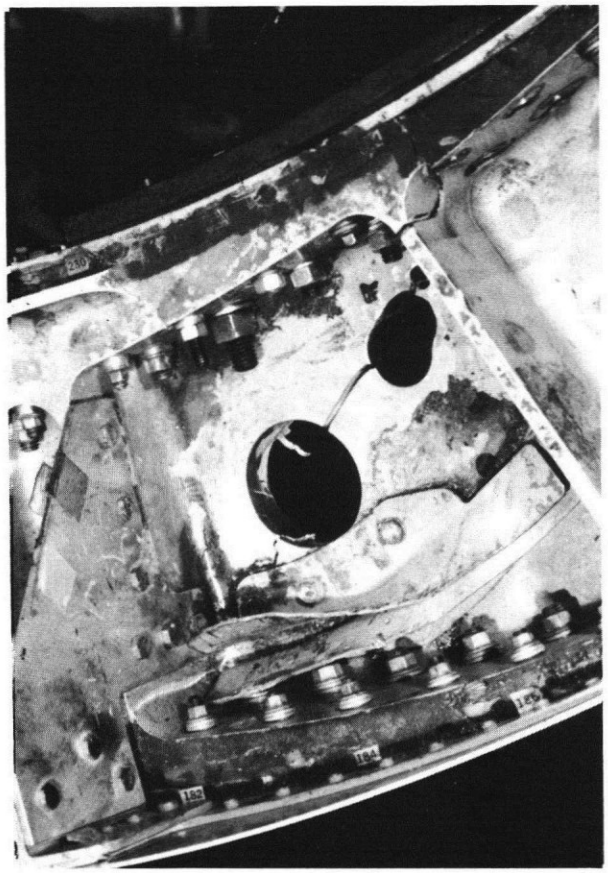

Figure 17. Final failure at the fuel pipe holes

The damage tolerance assessment of the JA-fin has involved testing of the main and forward attachments. In this paper the forward attachment is considered. The testing was made in two steps. Firstly, test specimens simulating the attachment lug were tested separately in a servo-hydraulic testing machine. The test specimens were designed on basis of FE-analyses of both the real attachment geometry and the test specimen configuration. Both geometry and stress distributions in a region of the lug correlated very well between the test specimen and the real attachment according to the analyses.

Crack growth from an electro-discharged corner defect was monitored visually. The first test specimen, simulating the lug, was spectrum fatigue tested for 11.4 design life times (DLT) resulting in a crack growth of 0.62 mm. After increasing the load level first to 1.176 times the design limit load (DLL) and later on to 1.5 times the DLL a crack growth of 2.20 mm was obtained in 38 DLT. Final failure occurred outside the test region.

The second identical test specimen was spectrum fatigue tested after precracking with constant amplitude loading. The constant amplitude precracking was a result of the slow crack growth in the first test specimen. Starting with a 5.25 mm corner crack (after precracking) 2.70 mm of crack growth under spectrum loading was recorded before crack arrest occurred after 19 DLT (no more crack growth was recorded during the following 6.9 DLT).

It is believed that the interference fitted ball bearing in the lug hole and the interference fitted bushing in the wing bolt hole, discussed above, restrain the crack mouth opening. This would reduce the effective stress intensity factor range and could be the explanation for the unexpectedly slow crack growth observed at these locations.

In the second step of the forward fin attachment testing the region outside the attachment lug was considered. In this test a complete fin was used to get the correct clamping of the attachment, see Figure 18. Prior to testing, two artificial defects were introdued at a stress concentration in the forward edge of the flange and at a fastener hole also in the flange of the attachment. Then spectrum testing without any observed crack growth for 2 DLT took place. Next, four more defects were introduced by sawing. The locations of all six defects are shown in Figure 19. Then a total of 6 DLT of spectrum loading was applied, still without any registration of crack growth. At this stage the four latest introduced defects were increased in size to enforce crack growth.

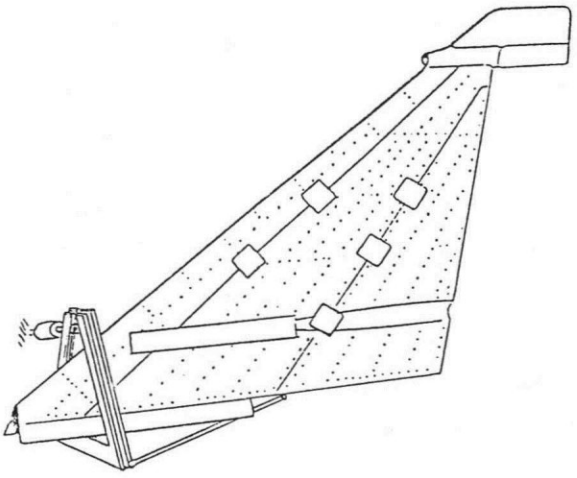

Figure 18. Test set-up for testing of JA 37 forward fin attachment

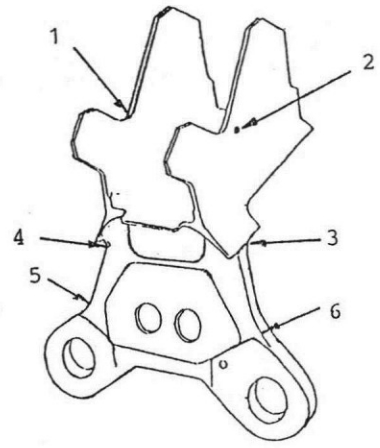

Figure 19. Forward fin attachment with initial flaw locations indicated

The load sequence consisted of 333 simulated flight hours and was repeated until failure occurred. The six largest loads (in magnitude) occur in three pairs of plus/minus a certain percentage of the DLL. Furthermore, these pairs occur rather closely in the beginning of the sequence. As can be expected, this led to significantly faster crack growth on the side of the attachment that was subjected to primarily tension/compression loads than on the opposite side which felt compression/tension loads. This detail of the load sequence manifested itself in that crack number 3, see Figure 19, which started from an artificially made flaw of 1.5 mm grew only 1.4 mm during 7330 flight hours. During the same time crack number 4 grew a total of 21.0 mm from a size of 4.0 mm.

Fractographic results clearly reveal the entire crack growth process for both crack number 3, Figure 20, and crack number 4, Figure 21.

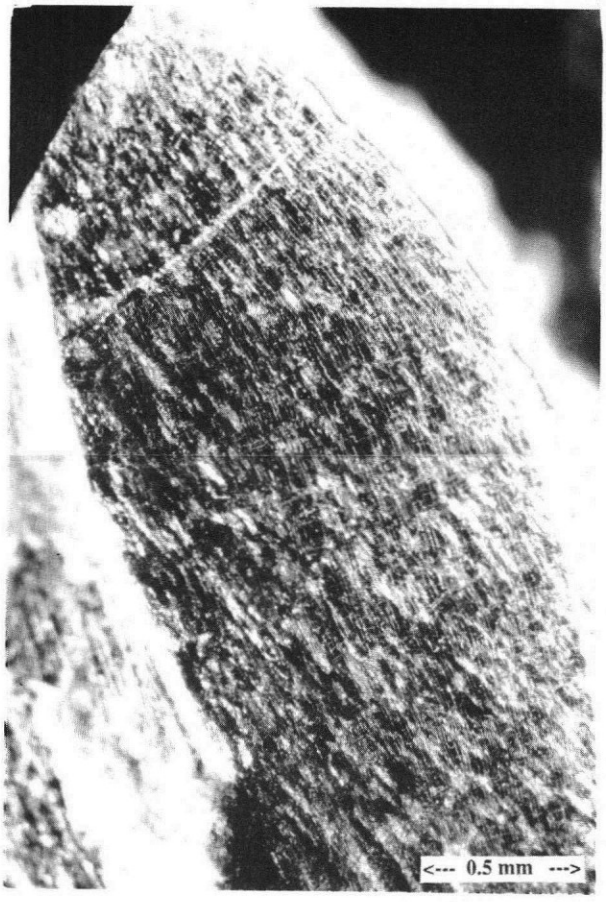

Figure 20. Crack surface of flaw No 3

Figure 21. Crack surface of flaw No 4

The fin will during real flights see a random sequence in which the peculiarity of the test sequence does not exist. Thus, actual crack growth would be somewhere between the extreme results obtained in the testing. For the most conservative case, crack number 4, a comparison between experimental and predicted crack growth is shown in Figure 22.

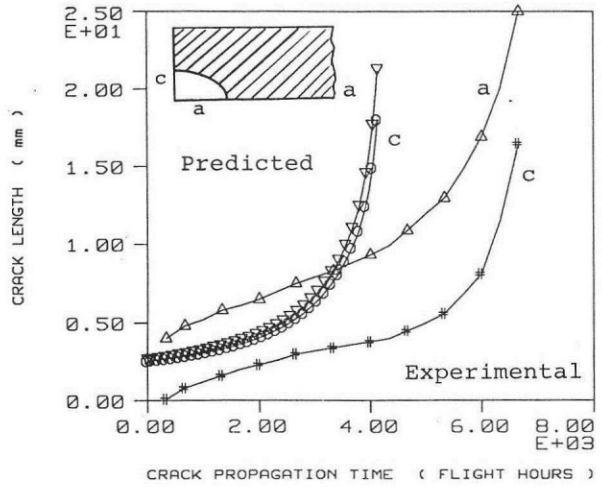

Figure 22. Comparison of measured and predicted crack propagation for flaw No 4.

Inspection Intervals

Based primarily upon crack growth predictions but with consideration of component testing results and results concerning the prediction capability (accuracy for various structural details) of the computer programme used safe periods of crack growth have been established. Inspection intervals have been determined, assuming that the critical locations are depot or base level inspectable. The inspection intervals are then half the periods of safe crack growth. Figures 23 and 24 show inspection intervals for the two components which have been focused upon in this paper.

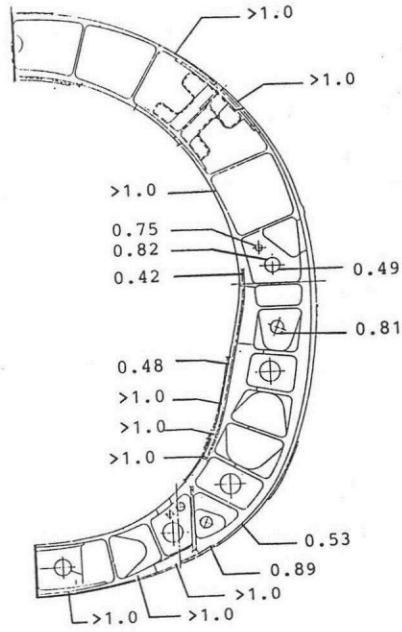

Figure 23. Suggested inspection intervals in design life times (DLT), to ensure damage tolerance

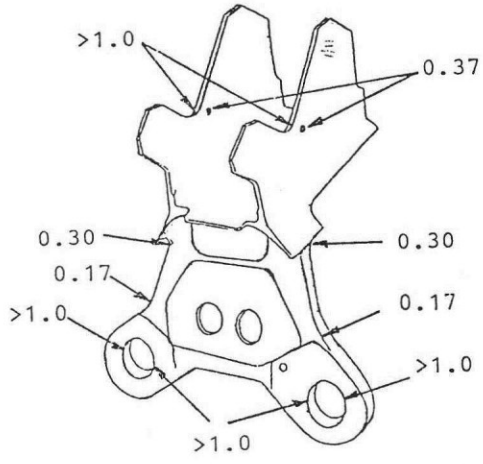

Figure 24. Suggested inspection intervals in design life times (DLT), to ensure damage tolerance of the forward fin attachment